WILEY-VCH

FULL PAPER

Ru water oxidation catalysts based on py_5 ligands

Marcos Gil-Sepulcre,[a,b] Michael Böhler,[c] Mauro Schilling,[c] Fernando Bozoglian,[a] Cyril Bachmann,[c] Dominik Scherrer,[c] Thomas Fox,[c] Bernhard Spingler,[c] Carolina Gimbert-Suriñach,[a] Roger Alberto,[c] Roger Bofill,[b] Xavier Sala,[b] Sandra Luber,* [c] Craig J. Richmond,[c] and Antoni Llobet*[a,b]

Abstract: Ru complexes containing the pentapyridyl ligand 6,6''-(methoxy(pyridin-2-yl)methylene)di-2,2'-bipyridine (L-OMe) of general formula *trans*-[Ru^{II}(X)(L-OMe-κ-N^5)]$^{n+}$ (X = Cl, n = 1, *trans*-**1**$^{+}$; X = H_2O, n = 2, *trans*-**2**$^{2+}$) have been isolated and characterized in solution (NMR, UV-Vis) and in the solid state by XRD. Both complexes undergo a series of substitution reactions at oxidation state II and III, when dissolved in aqueous triflic acid-trifluoroethanol solutions that have been monitored by UV-vis spectroscopy and their corresponding rate constants reported. In particular, aqueous solutions of the Ru^{III}-Cl complex *trans*-[Ru^{III}(Cl)(L-OMe-κ-N^5)]$^{2+}$ (*trans*-**1**$^{2+}$) generates a family of Ru-aqua complexes namely *trans*-[Ru^{III}(H_2O)(L-OMe-κ-N^5)]$^{3+}$ (*trans*-**2**$^{3+}$), [Ru^{III}(H_2O)$_2$(L-OMe-κ-N^4)]$^{3+}$ (*trans*-**3**$^{3+}$) and [Ru^{III}(Cl)(H_2O)(L-OMe-κ-N^4)]$^{3+}$ (*trans*-**4**$^{2+}$). While complex *trans*-**4**$^{2+}$ is a powerful water oxidation catalyst, complex *trans*-**2**$^{3+}$ has only a moderate activity and *trans*-**3**$^{3+}$ is not a catalyst. Further, a parallel work has been carried out with related complexes but containing the methyl substituted ligand 6,6''-(1-pyridin-2-yl)ethane-1,1-diyl)di-2,2'-bipyridine (L-Me). The behavior of all these catalysts has been rationalized based on substitution kinetics, oxygen evolution kinetics, electrochemical properties and DFT calculations. The best catalysts, *trans*-**4**$^{2+}$, reach turnover frequencies of 0.71 s^{-1} using Ce(IV) as a sacrificial chemical oxidant with oxidative efficiencies above 95%.

[a] M. Gil-Sepulcre, Dr. F. Bozoglian, Dr. C. Gimbert-Suriñach, and Prof. Dr. A. Llobet
Institute of Chemical Research of Catalonia (ICIQ), Av. Països Catalans 16, 43007 Tarragona (Spain)
E-mail: allobet@iciq.es

[b] M. Gil-Sepulcre, Dr. R. Bofill, Dr. X. Sala, and Prof. Dr. A. Llobet
Departament de Química, Universitat Autònoma de Barcelona
Cerdanyola del Vallès, 08193 Barcelona (Spain)

[c] M. Böhler, M. Schilling, Prof. Dr. S. Luber, Dr. C. Bachmann, D. Scherrer, Dr. T Fox, Prof. Dr. B. Spingler, Prof. Dr. R. Alberto and Dr. C. J. Richmond
Department of Chemistry B, University of Zurich, Winterthurerstrasse 190, CH-8057, Zurich, Switzerland.
E-mail: sandra.luber@chem.uzh.ch

Supporting information for this article is given via a link at the end of the document.

Introduction

The oxidation of water to give molecular oxygen together with the reduction of water to give molecular hydrogen, are the two key reactions involved in the water splitting process. If the energy required to perform the reaction comes from sunlight, this process becomes a sustainable way of producing a renewable fuel that may replace the fossil fuels in a future energy economy.[1] Both reactions require the use of catalysts that activate the water molecule and allow the formation of new O-O and H-H bonds. In the particular case of the water oxidation half-reaction, mononuclear and dinuclear ruthenium-polypyridyl complexes have been described that are very fast and efficient catalysts for this reaction.[2] Among them, those complexes containing one or two anionic carboxylate groups, have shown to give the best results in terms of overpotential and turnover frequency, in some cases reaching values over one million turnover numbers.[3] The high efficiency of these catalysts is attributed to the synergistic effect of several factors; i) stabilization of Ru high oxidation states by high sigma donation of the carboxylate anionic ligands, ii) the possibility to form seven coordinated ruthenium species at high oxidation states, iii) formation of intramolecular hydrogen bonds between the Ru-OH and the carboxylate groups, the latter acting as an auxiliary base. Other crucial contributions from the ruthenium-polypyridinic complexes research are the mechanistic studies of the water oxidation reaction, which shed some light into the catalytic pathways that lead to the formation of molecular oxygen.[4] Indeed, the investigation of the mechanism of the reaction, including electrochemical, kinetic studies, detection of key intermediates as well as theoretical calculations, are essential for a rational design of new and better catalysts.

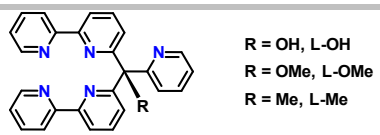

Chart 1. Ligands discussed in this work.

In this work, two new ruthenium complexes coordinated by the pentapyridine ligand 6,6''-(methoxy(pyridin-2-yl)methylene)di-2,2'-bipyridine, L-OMe in Chart 1, are prepared. The two compounds differ in the sixth coordination ligand, which is either a chlorido ligand or an aquo ligand. A comprehensive kinetic analysis of the ligand-aquo substitution reactions that generate the active species for each compound is described and their capacity to oxidize water into oxygen gas is evaluated. The kinetics and catalytic results are compared with those obtained for analogous complexes containing the methyl derivative ligand 6,6''-(1-pyridin-2-yl)ethane-1,1-diyl)di-2,2'-bipyridine, L-Me in Chart 1. Density functional Theory (DFT) calculations of intermediate species and key transition states support the experimental results.

Results and Discussion

Synthesis and structural characterization of complexes 1^+ and 2^{2+}

Complex [Ru(L-OMe)Cl]$^+$, **1**$^+$, was prepared from ligand L-OH shown in Chart 1, after methylation of the OH group and *insitu* complexation with $RuCl_3$ (Scheme 1). The reaction gave a 2:1 mixture of the *trans*-**1**$^+$ and *cis*-**1**$^+$ isomers that can be clearly identified in the ^{1}H NMR spectrum of the reaction crude mixture (Figure S2 in SI, here *trans* and *cis* refer to the relative disposition of the pyridine (in blue) and chlorido ligands as indicated in Scheme 1). A pure sample of the *trans*-**1**$^+$ isomer was isolated in 35 % yield after column chromatography and recrystallization. A *trans* and *cis* mixture is also obtained for the related complex **1'**$^+$ containing a methyl group instead of a methoxy group attached to the C-sp^3 atom of the pentapyridyl ligand (L-Me in Chart 1).[5] The Ru-aquo complex *trans*-[Ru(L-OMe)(OH_2)]$^{2+}$, *trans*-**2**$^{2+}$, was prepared in 65 % yield from *trans*-**1**$^+$ after reaction with $AgNO_3$ that removes the Cl-ligand from the first coordination sphere and promotes aquation (Scheme 1).

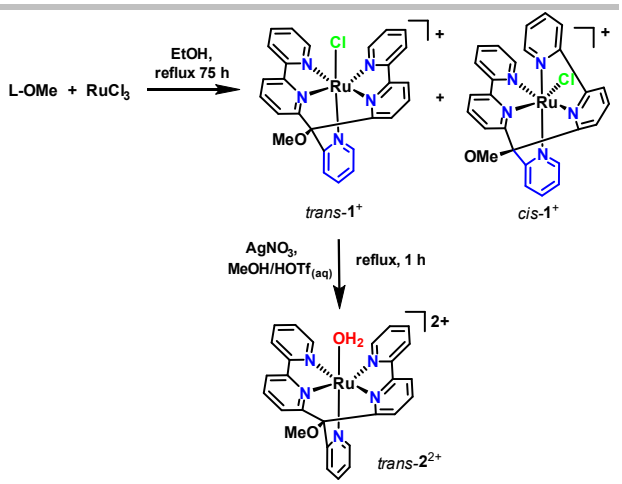

Scheme 1. Synthesis of complexes *trans*-**1**$^+$ and *trans*-**2**$^{2+}$ discussed in this work.

Complexes *trans*-**1**$^+$ and *trans*-**2**$^{2+}$ have been characterized by NMR, mass spectrometry and elemental analysis. The ^{1}H NMR spectra of both complexes show one single set of signals for the two bipyridyl groups, as expected according to the symmetry of the trans isomer. Good quality crystals, suitable for single crystal x-ray diffraction studies, were obtained for both complexes. Figure 1 shows the representative molecular structure of the chlorido complex *trans*-**1**$^+$. The Ru complex has a distorted octahedral geometry due to the steric constrains imposed by the pentadentate L-OMe ligand, resulting in a Cl-Ru-N_{pyr} angle of

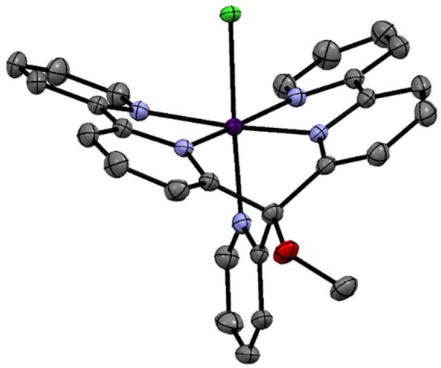

170.0º. The rest of the bond distances and angles are within expected values for related octahedral ruthenium complexes containing polypyridine ligands.[5,6] It is interesting to observe that the angle between the two bipyridyl groups of L-OMe situated in the equatorial plane is 134.4º as opposed to the 180º expected for an ideal octahedron with no restraints between the bipyridyl ligands. This is due to constraints imposed by the sp^3 carbon atom connecting the two bipyridyl groups. Similar structural characteristics are observed for the analogous aquo complex *trans*-**2**$^{2+}$ (Figure S10 in SI).

Figure 1. ORTEP representation of *trans*-**1**$^{+}$ at 50% probability level. The counter ions, solvent molecules and hydrogen atoms have been omitted for clarity. Colour code: C, grey; N, blue; O, red; Cl, green; Ru, purple.

DFT calculations were also carried out to complete the structural characterization of the complexes described, as well as to shed light into key intermediates and transition states involved in the catalytic cycle. Good structural agreement was found between structures obtained from geometry optimization with DFT using BP86[7]-D3[8]/def2-TZVP[9] and the crystallographic data. The M06-L[10] functional and the PBEh-3c method[11] (based on the PBE functional[12]) were also tested and gave similar results for the experimentally verifiable structures. Electronic energies were obtained with B3LYP[13]-D3/def2-TZVP/COSMO[14] and were practically identical to those obtained with PBE0 (PBE0-D3/def2-TZVP/COSMO) which has been recommended by Kang *et al.*[15] Unless otherwise noted, energies are reported as free energies consisting of electronic energies plus energy corrections from the solvation model (B3LYP-D3/COSMO) and thermal corrections obtained with the BP86 exchange-correlation functional (for details, see SI). We note that the complexes were modelled with the methoxy group being 'anti' to the pyridine fragment ('gauche' in crystal structures) because the rotational barrier for the isomerization was small and subsequent structures showed a preference for the 'anti' isomer.

The *trans* isomer of **1**$^{+}$ is approx. 1.0 kcal mol^{-1} more stable than its *cis* counterpart, which is in agreement with *trans*-**1**$^{+}$ being the major compound in the synthetic mixture, under the assumption that the reaction conditions lead to an equilibrium mixture. For the oxidized isomers *trans*-**1**$^{2+}$and *cis*-**1**$^{2+}$ we find a free energy difference of about 0.7 kcal mol^{-1}, which is in very good agreement with the experimental value as well as discussed below. Although such small computed energy differences in general need to be taken with caution, we note that said complexes show a high degree of structural similarity which supports a high level of error cancellation.

Low oxidation states: substitution and isomerization reactions

We studied the reactivity of complexes *trans*-**1**$^{+}$ and *trans*-**2**$^{2+}$ towards aquo substitution and oxidation reactions by time resolved UV-Visible spectroscopy. For fast processes ($t_{½}$ < 170 sec) stopped-flow techniques were employed. The rate constants were calculated using Reactlab Kinetics simulation software. Species distribution diagrams and simulated spectra were obtained with the same software. Cyclic voltammetry (CV) and Differential Pulse Voltammetry (DPV) techniques were used to study the redox properties of all the complexes described here. All potentials reported are given *vs*. the NHE electrode. In addition, we used Density Functional Theory (DFT) calculations to obtain theoretical redox potentials and key transition states to support our experimental results. Details about the experimental procedures and calculations are given in the supporting information (SI).

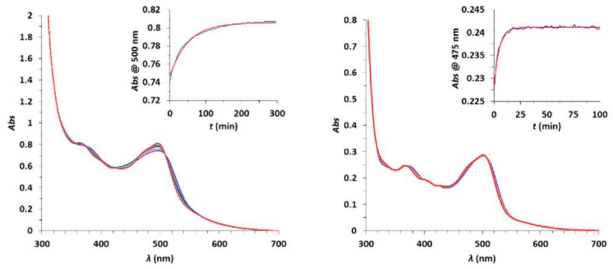

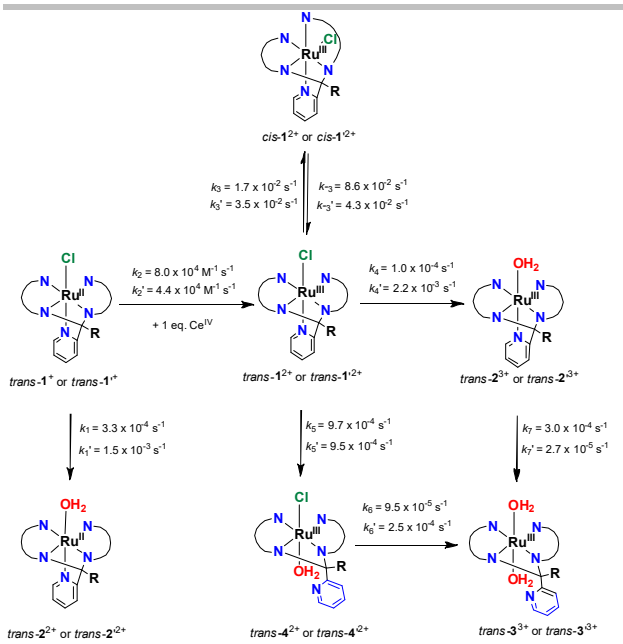

Scheme 2. Reaction pathways associated with *trans*-**1**$^{+}$ and *trans*-**1'**$^{+}$ containing the L-OMe and L-Me ligands, respectively. The latter complexes and their associated kinetic constants are denoted with a prime.

The kinetics of the conversion of the chlorido complex *trans*-**1**$^{+}$ to the aquo complex *trans*-**2**$^{2+}$ in aqueous 0.1 M trifluoromethansulfonic acid:trifluoroethanol solution (TfOH:TFE, 95:5) was studied using a 40 μM solution of *trans*-**1**$^{+}$ and monitored via UV-vis spectroscopy (Figure 2, left). TFE was used to increase the solubility of the complex. The final spectra matched that of isolated *trans*-**2**$^{2+}$ (Figure S9, SI). The substitution reaction is relatively slow, showing a pseudo-first order rate constant of k_1 = 3.3 x 10^{-4} s^{-1} and half time of $t_{½}$ = 35 min (see bottom left of Scheme 2). In sharp contrast, the same reaction for the analogue *trans*-**1'**$^{+}$ containing the L-Me ligand is one order of magnitude faster under the same conditions with a rate constant of k_1' = 1.5 x 10^{-3} s^{-1} and half time of $t_{½}$ = 8 min (Figure 2, right). The chlorido to aquo substitution at oxidation state Ru(II) is also evident from CV experiments of *trans*-**1**$^{+}$ in an aqueous mixture of 0.1 M TfOH:TFE. The intensity of the Ru(III/II) redox couple of the chlorido complex *trans*-**1**$^{+}$ at $E_{1/2}$ = 0.93 V slowly decreases when the solution is left standing for 30 minutes, while a new redox couple at higher potential $E_{1/2}$ = 1.12 V appears. This value matches the potential of the Ru(III/II) couple for the isolated aquo complex *trans*-**2**$^{2+}$ (Figure S17-S18 in SI). Calculated Ru(III/II) redox potentials using DFT reproduce the experimental results well, giving values of 0.8 V (0.93 V experimental value) and 1.3 V (1.12 V experimental value) for the chlorido and aquo complexes, respectively (Figure S24-S25 in the SI).

Figure 2. Evolution of UV-vis absorption spectra over time of a 40 μM solution of *trans*-**1**$^{+}$ (left) and *trans*-**1'**$^{+}$ (right) in 0.1 M TfOH solution containing 5% of TFE at 25 °C. The inset figures show the experimental kinetics profile at a specific wavelength (blue) and its mathematical fit (red).

We then explored the substitution reactions upon one electron oxidation of *trans*-**1**$^{+}$ with cerium (IV) ammonium nitrate (Ce(IV) hereafter). The fast outer sphere electron transfer reaction between Ce(IV) and *trans*-**1**$^{+}$ to give *trans*-**1**$^{2+}$ was followed by stopped-flow UV-Vis spectroscopy and fitted to a second order kinetic profile with a rate constant of k_2 = 8.0 x 10^{4} M^{-1} s^{-1} (Figure 3 and Scheme 2, center left). Following the formation of the oxidized complex *trans*-**1**$^{2+}$, a second slower process was observed in the stopped-flow experiment, which corresponds to the isomerization of *trans*-**1**$^{2+}$ to *cis*-**1**$^{2+}$ that remain in equilibrium as indicated in the top part of Scheme 2. The final distribution of species was calculated by means of ^{1}H NMR analysis of a solution of *trans*-**1**$^{+}$ after oxidation with Ce(IV) and re-reduction with sodium ascorbate (Figure S13 in SI). The kinetic constants for this process were calculated to be k_3 = 1.7 x 10^{-2} s^{-1} and k_{-3} = 8.6 x 10^{-2} s^{-1}. A species distribution diagram is shown in Figure 3 that shows that the equilibrium is reached within a few seconds giving a final *trans* and *cis* mixture of *ca.* 9:1. A parallel isomerization process was observed for the methyl derivative *trans*-**1'**$^{+}$ but the final equilibrium gives a calculated distribution of

trans-**1'**$^{2+}$ and *cis*-**1'**$^{2+}$ in 3:2 ratio and rate constants of k_3' = 3.5 x 10^{-2} s^{-1} and k_{-3}' = 4.3 x 10^{-2} s^{-1} (Figure S12 and S14 in SI).

Figure 3. (Top) (Left) Evolution of stopped-flow UV-vis absorption spectra of a 63 μM solution of *trans*-**1**$^{+}$ with 1 equivalent of Ce(IV) in 0.1 M TfOH solution containing 5% of TFE at 25 °C for one minute. *Inset.* Evolution spectra of the first process (1 second) attributed to the oxidation of *trans*-**1**$^{+}$ to *trans*-**1**$^{2+}$. (Right) changes in the absorbance at 500 nm vs time for one minute (blue line) and its

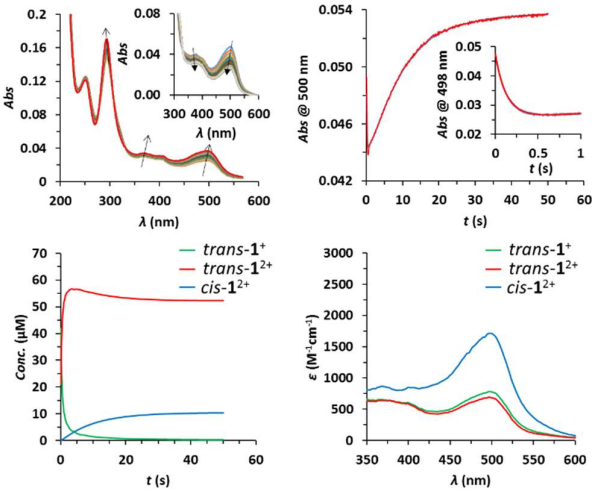

mathematical fit (red line). *Inset.* Changes in the absorbance at 498 nm vs time (blue line) and its mathematical fit (red line), during 1 second of reaction. **(Bottom)** (Left) calculated concentration distribution diagram vs time for the different species. (Right) calculated spectra for the proposed species in solution.

At longer oxidation reaction times, we observed a complex kinetics profile, which indicates that several processes are taking place in the mixture (Figure 4, top). As indicated in Scheme 2, the key intermediate species *trans*-**1**$^{2+}$ can undergo labile chlorido ligand substitution to give the Ru-aqua *trans*-**2**$^{3+}$ (Scheme 2, center right). Alternatively, it is possible that the aquo ligand replaces the pyridine giving rise to a trans chlorido-aquo-Ru complex with a dangling pyridine group (*trans*-**4**$^{2+}$ in Scheme 2, center bottom). The latter process is consistent with electrochemical results and DFT calculations obtained for trans-**1'**$^{2+}$, which demonstrated that the pyridine group in this type of complexes is prone to decoordination.[5] Indeed, cyclic voltammetry experiments of *trans*-**1**$^{+}$ in *dichloromethane* show an irreversible Ru(III/II) redox couple at E_{ox} = 1.11 V that gives rise to a new wave at $E_{1/2}$ = 0.53 V, associated with a trans-bis(chlorido) species with a pendant pyridine group as similarly observed for complex *trans*-**1'**$^{+}$ (Figure S19).[5] This process is favored by the release of strain upon pyridyl decoordination in both ligands L-OMe and L-Me.

The transient mono-aquo species *trans*-**2**$^{3+}$ and *trans*-**4**$^{2+}$, both evolve to the bis-aquo complex *trans*-**3**$^{3+}$ species after a second substitution (Scheme 2, bottom right). This process was studied independently for complex *trans*-**2**$^{3+}$, which could be prepared from the one-electron oxidation of *trans*-**2**$^{2+}$ with Ce(IV) (Figure 5). The mathematical fit gives pseudo-first order kinetic

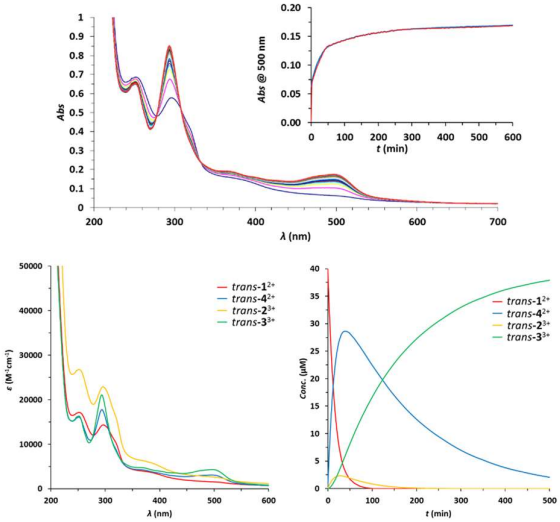

constant of k_7 = 3.0 x 10^{-4} s^{-1}. Cyclic voltammetry experiments in aqueous 0.1 M TfOH:TFE mixtures also show the formation of the bis(aquo) species *trans*-**3**$^{3+}$ with a characteristic Ru(III/II) couple at $E_{1/2}$ = 0.73 V, typical for this type of complexes (Figure 6 and Figures S17-S18 in SI).[16]

Figure 4. (Top) Evolution of UV-vis absorption spectra of a 40 μM solution of *trans*-**1**$^{+}$ with 1 equivalent of Ce(IV) in 0.1 M TfOH containing 5% TFE at 25 °C. *(inset)* Changes in abs. *vs*. t at 500 nm (blue line) and mathematical fit (red line). **(Bottom)** (Left) calculated spectra of the different species proposed in Scheme 2. (Right) calculated concentration distribution diagram *vs*. time for the different species.

The values of the remaining rate constants involved in the reaction sequence model indicated in Scheme 2 were calculated

by fixing the values of k_1, k_2, k_3, k_{-3} and k_7 obtained independently as discussed above. Thus, k_5 and k_4, assigned to two competitive reactions from the *trans*-**1**$^{2+}$ intermediate to form the corresponding Ru-aqua species *trans*-**4**$^{2+}$ and *trans*-**2**$^{3+}$, give values of k_5 = 9.7 x 10^{-4} s^{-1} and k_4 = 1.0 x 10^{-4} s^{-1} respectively. Once the Ru^{III}-Cl complex, *trans*-**1**$^{2+}$, is formed then the formation of the Ru-H_2O-Cl is the dominant species. Finally, at longer timescales, the bis-aqua *trans*-**3**$^{3+}$ complex forms from *trans*-**4**$^{2+}$, with a rate constant of k_6 = 9.5 x 10^{-5} s^{-1}.

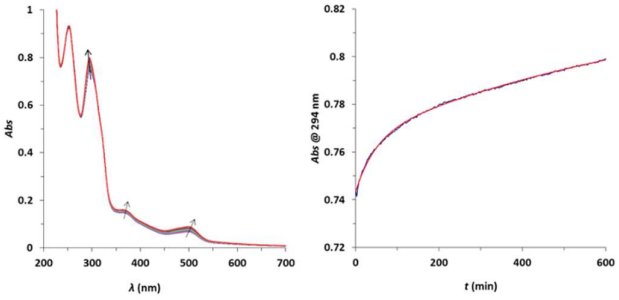

Figure 5. (Left) evolution of UV-vis absorption spectra at 25 °C of a 40 μM of *trans*-**2**$^{3+}$ in 0.1 M triflic acid solution containing 5% of TFE. (Right) changes in the absorbance at 294 nm vs time (blue line) and its mathematical fit (red line).

Figure 4 (bottom) shows the evolution of all the species derived from *trans*-**1**$^{2+}$ together with their respective UV-Vis calculated spectra. A comparison of the experimental UV-Vis spectrum of *trans*-**2**$^{3+}$ with its calculated spectrum shows a close match that gives a strong support to this reaction model (Figure S15 in SI). The same experiment and calculations were done for the methyl derivative *trans*-**1'**$^{2+}$ (Figure S16 in the SI). Although both complexes follow the same reaction scheme, the changes in kinetic constants have a dramatic effect on the relative distribution of species, particularly for the mono-aquo intermediates *trans*-**2**$^{3+}$ and *trans*-**4**$^{2+}$, both catalytically active species towards the water oxidation reaction. While the chlorido-aquo species *trans*-**4**$^{2+}$ is the major species in solution during the first minutes, the contribution of the *trans*-**2**$^{3+}$ is almost negligible (blue and yellow lines in Figure 4, respectively). For instance, we obtain a *trans*-**4**$^{2+}$:*trans*-**2**$^{3+}$ ratio of 92:8, 20 min after mixing *trans*-**1**$^{+}$ with Ce(IV). In contrast, an opposite trend is observed for the methyl derivative *trans*-**1'**$^{+}$, for which we observe a *trans*-**4'**$^{2+}$:*trans*-**2'**$^{3+}$ ratio of 26:74 at the same reaction time (Figure S16 in SI). These differences are crucial to understand the differentiated catalytic activity observed when the Ru-Cl complexes *trans*-**1**$^{+}$ and *trans*-**1**$^{+'}$, that are not water oxidation catalysts but catalyst precursors, are dissolved in aqueous mixtures of TfOH:TFE.

DFT calculated standard reduction potentials are in qualitative agreement with the CV data. Reduction potentials for the redox couple of Ru(III/II) of 0.8 V (exp. 0.92 V) for *trans*-**1**$^{2+}$/*trans*-**1**$^{+}$ and 1.3 V (exp. 1.12 V) for *trans*-**2**$^{3+}$/*trans*-**2**$^{2+}$ were found. Although the thermodynamic tables of both complexes show virtually identical values (see Figures S25 and S27 in the SI), it is the association of water (and the displacement of pyridine) in which they differ, in agreement with the experimental description. The displacement of pyridine by a water molecule is predicted to be endergonic for both ligands with the ruthenium metal center in the oxidation states II or III. The associated free energies are 4 and 1 kcal mol^{-1} for L-OMe (*trans*-**1**$^{+}$), and 14 and 12 kcal mol^{-1} for L-Me (*trans*-**1'**$^{+}$), respectively. Reflecting the experimental observation, the displacement is consistently calculated to be more endergonic (by approx. 10 kcal mol^{-1}) for the complex with the L-Me ligand compared to the one with the L-OMe ligand.

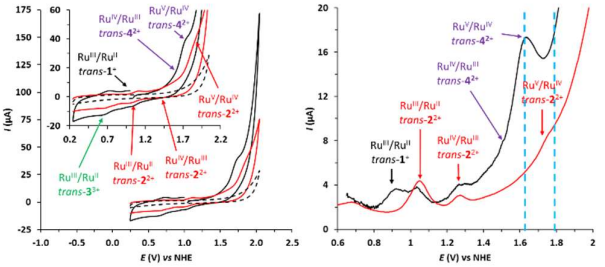

High oxidation states: water oxidation catalysis

CV and DPV experiments of the Ru-aquo complex *trans*-**2**$^{2+}$ in an aqueous mixture of 0.1 M TfOH:TFE (95:5) show the redox couples Ru(III/II) at $E_{1/2}$ = 1.12 V, Ru(IV/III) at $E_{1/2}$ = 1.28 V and Ru(V/IV) at $E_{1/2}$ ≈ 1.73 V, followed by a catalytic wave associated with water oxidation catalysis (Figure 6, red line). In the reverse scan in the CV, we also observe the characteristic Ru(III/II) redox couple at $E_{1/2}$ = 0.73 V associated with *trans*-**3**$^{3+}$, that is formed after oxidation (*vide supra*).

Figure 6. Cyclic Voltammograms (left) and Differential Pulse Voltammograms (right) of *trans*-$\mathbf{2}^{2+}$ (solid red) and *trans*-$\mathbf{1}^{+}$ measured 15 minutes after oxidation with 1 equivalent of Ce(IV) (solid black) in 0.1 M TfOH solution containing 5% of TFE. The addition of Ce(IV) generates four electroactive species in solution that are observed in the CV namely, *trans*-$\mathbf{1}^{2+}$:*trans*-$\mathbf{2}^{3+}$:*trans*-$\mathbf{3}^{3+}$:*trans*-$\mathbf{4}^{2+}$ in a 5:1:1:10 ratio; see text for details. The arrows indicated the assigned redox couple for the different species. Blue vertical lines in the DPV correspond the Ru(V)/R(IV) couple for *trans*-$\mathbf{2}^{3+}$ and *trans*-$\mathbf{4}^{2+}$, that is associated with water oxidation electrocatalysis. Dashed black correspond to a blank with no catalyst. Conditions: scan rate of 100 mV s^{-1}, [**Complex**] = 0.3 mM. Glassy Carbon disk as working electrode, Pt disk as counter electrode and $Hg/HgSO_4$ as reference electrode.

CV and DPV were also carried out, 15 minutes after the addition of Ce(IV) to a solution of *trans*-$\mathbf{1}^{+}$ and is shown in the black traces in Figure 6. According to the previous kinetic analysis this generates a mixture of one Ru(III)-Cl complex and three Ru(III)-aqua complexes with the following ratios: *trans*-$\mathbf{1}^{2+}$:*trans*-$\mathbf{2}^{3+}$:*trans*-$\mathbf{3}^{3+}$:*trans*-$\mathbf{4}^{2+}$ of 5:1:1:10. Ru-aqua complexes *trans*-$\mathbf{2}^{3+}$ and *trans*-$\mathbf{3}^{3+}$ have been characterized independently and thus simplifies the assignment shown in Figure 6. The most interesting feature that is observed in the Figure is the 200 mV cathodic shift of the electrocatalytic wave with regard to that of *trans*-$\mathbf{2}^{3+}$ (see the blue vertical lines in the DPV in Figure 6), and large enhancement of the catalytic current density under comparable conditions. This significant negative shift of the onset of the catalysis is a consequence of the higher electron density transmitted by the anionic chlorido ligand to Ru in *trans*-$\mathbf{4}^{2+}$ as compared to the pyridyl group in *trans*-$\mathbf{2}^{3+}$, that highly stabilizes Ru(V). The large enhancement in kinetics is associated with the dangling pyridyl ligand in *trans*-$\mathbf{4}^{2+}$ that acts as base and accepts a proton at the O-O bond formation step during the water nucleophilic attack as will be further discussed below. The contribution from *trans*-$\mathbf{2}^{3+}$ in this case is negligible due to the much lower concentration and activity.

The same striking differences are observed on manometric experiments monitoring the oxygen evolution profiles obtained after chemically induced catalysis. Indeed, addition of 100 equivalents of Ce(IV) to a 1 mM complex solution (black and blue lines in Figure 7) shows that while the *trans*-$\mathbf{2}^{2+}$ complex gives modest turnover numbers (TONs) of 8 and initial turnover frequency (TOF_i) of 0.037 s^{-1}, the complex *trans*-$\mathbf{4}^{2+}$ (generated by the addition of Ce(IV) to the Ru-Cl complex *trans*-$\mathbf{1}^{+}$) gives 24 TONs that represents a 96% oxidative efficiency based on Ce(IV) with a TOF_i = 0.71 s^{-1} (20 times faster; see Table 1). Lowering the catalyst concentration to 1 μM increases the TONs up to 168 but lowers the oxidative efficiency to 67% (Figure S22 in SI). A second and third subsequent additions of Ce(IV) to the catalytic mixture generated upon dissolving *trans*-$\mathbf{1}^{+}$, shows that the system is still active with oxidative efficiencies higher than 95% (Figure S23 in SI). However, the slopes of the catalytically generated oxygen over time decrease after each addition of Ce(IV). This is a phenomenon that is attributed to the increased concentration of nitrate ions in solution due to the successive addition of Ce(IV), as observed before for related catalytic systems.[17] Another deactivation pathway that might be occurring is the conversion of *trans*-$\mathbf{1}^{+}$ to *trans*-$\mathbf{2}^{2+}$ in aqueous solutions at longer periods of time that we have shown to occur in the previous section. Indeed, when analogous manometry experiments using *trans*-$\mathbf{1}^{+}$ were performed a few minutes after catalyst mixing, the catalytic activity dropped to give similar results to those obtained

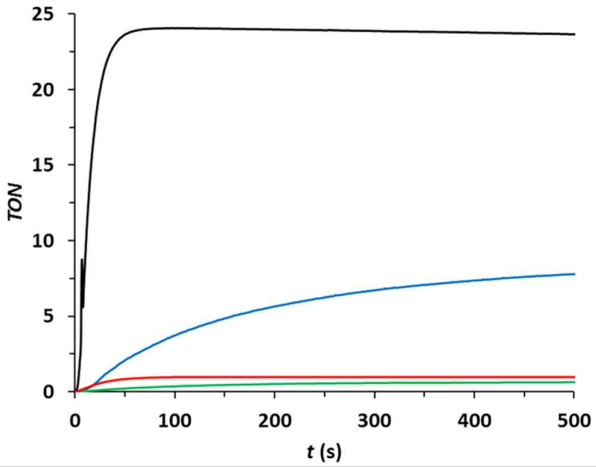

for the Ru-aquo complex *trans*-**2**$^{2+}$, in agreement with the kinetic analysis described in the previous section.

Figure 7. Oxygen evolution profile, given in turnover numbers (TON) *vs.* time for complex *trans*-**4**$^{2+}$ (generated from the *in situ* addition of Ce(IV) to *trans*-**1**$^{+}$; black line), *trans*-**2**$^{2+}$ (blue line), *trans*-**2'**$^{2+}$ (red line) and generated in situ from *trans*-**1'**$^{+}$ (green line). Conditions: 1 mM catalyst or precursor catalyst in 0.1 M TfOH solution (pH 1) and 100 equivalents of Ce(IV) at 25 °C.

The coordination environment of complex *trans*-**2**$^{2+}$, is reminiscent to that of [(trpy)(bpy)Ru(H$_2$O)]$^{2+}$, **5**$^{2+}$, and [(trpy)(Hbpp)Ru(H$_2$O)]$^{2+}$, **6**$^{2+}$, complexes (where trpy = 2,2':2",6'-terpyridine, bpy = 2,2'-bipyridine, Hbpp = 2,2'-(1Hpyrazole-3,5-diyl)dipyridine) in the sense that they are coordinated by five neutral pyridyl groups besides the critical aqua ligand. In agreement with this analogous coordination environment the Ru(V/IV) redox potential of *trans*-**2**$^{2+}$, **5**$^{2+}$ and **6**$^{2+}$ (1.7-1.8V range) and their catalytic water oxidation activities are similar.[18] In sharp contrast the 20 times increase in rate and the nearly 100% oxidative efficiencies for *trans*-**4**$^{2+}$ as compared to *trans*-**2**$^{2+}$, is associated with the presence of both the coordinated chlorido group au lieu of the pyridyl group, in *trans*-**2**$^{2+}$ and in **5**$^{2+}$, and the presence of the dangling pyridyl moiety as mentioned earlier.

Table 1. Summary of catalytic performance of complexes *trans*-**4**$^{2+}$, *trans*-**2**$^{2+}$, *trans*-**1'**$^{+}$ and *trans*-**2'**$^{2+}$. Conditions: 1 mM catalyst in 0.1 M TfOH solution (pH 1) and 100 equivalents of Ce(IV) at 25 °C.

Complex	TON	Ox. Eff.[b] (%)	TOF$_i$[c] x10^3
trans-**4**$^{2+}$,[a]	24	96	710
trans-**2**$^{2+}$	8	32	37
trans-**1'**$^{+}$	0.67	2.7	4
trans-**2'**$^{2+}$	1	4	21

[a] Obtained from the addition of Ce(IV) to *trans*-**1**$^{+}$. [b] Ox. Eff. = oxygen efficiency = (measured mols O_2)/(theoretical mols O_2). Calculated from manometry and on-line mass spectrometry experiment. [c] Initial turnover frequencies in s^{-1}.

Interestingly, the related complex *trans*-**1'**$^{+}$, shows a completely different scenario. Oxygen evolution experiments after addition of Ce(IV) to solution of the chlorido *trans*-**1'**$^{+}$ and aquo *trans*-**2'**$^{2+}$ complexes both show a very poor catalytic activity with 1 TON or less (Figure 7 and Table 1). This result is consistent with the relative concentration of active species extracted from the species distribution diagram based on the substitution kinetics described earlier (see Figure S16 in the SI). Here the corresponding highly active chlorido-aquo complex *trans*-**4'**$^{2+}$ is a minor species in the mixture whereas the modestly active mono-aquo complex *trans*-**2'**$^{3+}$ is the major compound.

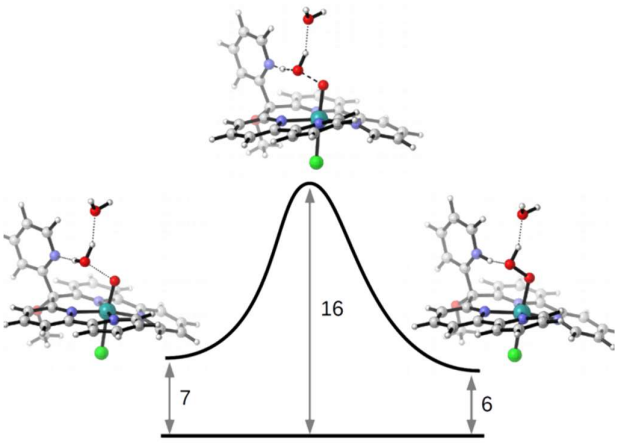

Figure 8. DFT calculated energy diagram of the nucleophilic attack of a water molecule to the Ru=O species derived from *trans*-**1**$^{+}$ to form a Ru-OOH species. The values are given in kcal mol^{-1} with respect to the separated reactants.

As previously mentioned the DFT calculated standard reduction potentials for the Ru(III/II) redox couple are in qualitative agreement with the CV data. In contrast to this, the computed reduction potentials for the Ru(IV/III) and Ru(V/IV) couples derived from *trans*-**2**$^{2+}$ are substantially higher than the ones obtained in CV measurements. This might be a failure of the implicit solvation model and may, for instance, be mitigated via a wider correlation of computed and experimentally determined redox potentials. Additionally, we note that test calculations using

the DCOSMO-RS[19] and SMD[20] solvation models predict similar values. Despite the flaws in the above case, the calculated reduction potential of 1.8 V for the Ru(V/IV) couple of, $[Ru(O)(Cl)(L\text{-}OMe\text{-}\kappa\text{-}N^4)]^+$, is supported by the experimental value of 1.62 V (extracted from DPV in Figure 6) and validates at least qualitative statements regarding trends in activity. For *trans*-$\mathbf{2}^{2+}$ a significantly higher reduction potential (600 mV shift) compared to the chlorido containing species is obtained (as can be expected from its higher charge, Figures S24-S25 in the SI).

Transition states energies for the WNA in the Ru(V) oxidation state for complexes with both ligand frameworks (L-OMe and L-Me) are practically identical. They are computed to be 16 and 14 kcal mol^{-1} with respect to the separated reactants for the OMe and Me ligands, respectively (Figures 8 and S27). The transition states were modelled with an explicit solvent water molecule as the corresponding peroxido species could not be found otherwise. The role of the dangling pyridine as a proton acceptor can be observed in these structures. A similar transition state for the aquo complex with two explicit water molecules, where one water molecule would act as the base, could not be obtained. Modelling with more water molecules was not further pursued in this study.

Conclusions

A detailed kinetic study of the ligand substitution reactions of ruthenium complexes *trans*-$\mathbf{1}^{+}$ and *trans*-$\mathbf{2}^{2+}$ by water, in aqueous solution, reveal a multiple reaction sequence involving both the chlorido and one pyridyl group of the pentapyridyl ligand L-OMe. The same reactions are observed for related complexes *trans*-$\mathbf{1'}^{+}$ and *trans*-$\mathbf{2'}^{2+}$ containing the ligand L-Me. However, the differences on the kinetic constant values of the consecutive steps generate a distinct distribution of intermediate species for *trans*-$\mathbf{1'}^{+}$ as compared to *trans*-$\mathbf{1}^{+}$. Thus, for the L-OMe complex *trans*-$\mathbf{1}^{+}$ the major species in solution during the first minutes is the chlorido-aquo complex *trans*-$\mathbf{4}^{2+}$. In contrast, the aquo complex *trans*-$\mathbf{2'}^{3+}$ is the most abundant species for *trans*-$\mathbf{1'}^{+}$. These differences are responsible for dramatic changes in their water oxidation catalytic activity as observed by electrochemical, oxygen evolution experiments and DFT calculations. Our computational analysis suggests that the formation of the active *trans*-$\mathbf{4}^{2+}$-type complex is the crucial step in the catalytic cycle and is mainly responsible for the different activities, since subsequent steps (PCETs, oxidations, WNA) show virtually identical free energies in both systems. This could be used as a handle to improve such catalysts. Complex *trans*-$\mathbf{4}^{2+}$ is a fast catalyst that operates with TOF_i = 0.71 s^{-1} and produces 168 TON in the presence of 1000 equivalents of Ce(IV) as sacrificial agent. On the other hand, complexes *trans*-$\mathbf{2}^{2+}$ and *trans*-$\mathbf{2'}^{+}$ are poor catalysts producing less than 8 and 1 TONs respectively. Eventually, both catalysts evolve to the inactive bis(aquo) complexes *trans*-$\mathbf{3}^{3+}$ and *trans*-$\mathbf{3'}^{3+}$.[21] The difference in the catalytic performance of *trans*-$\mathbf{4}^{2+}$ and *trans*-$\mathbf{2}^{3+}$ is due to the chlorido ligand in *trans*-$\mathbf{4}^{2+}$ that helps in lowering the redox potential to access Ru(V) that is the species responsible for electrocatalysis, and in the presence of the pendant pyridine group facilitates the O-O bond formation step, lowering the kinetic barrier at the water nucleophilic attack step.

Acknowledgements

MINECO and FEDER (CTQ2016-80058-R, CTQ2015-64261-R, CTQ-2015-73028-EXP, SEV 2013-0319, ENE2016-82025-REDT, CTQ2016-81923-REDC) and AGAUR (2014-SGR-915). The authors thank the *University of Zurich* and the *URPP LightChEC* for financial support as well as the *Swiss National Supercomputing Center* (project id: s425 and s745) for computational resources. S.L. acknowledges funding by the *Swiss National Science Foundation* (grant No. PP00P2_170667). Laurent Moser is also acknowledged for his assistance in the synthesis of complex $\mathbf{1}^{+}$.

Keywords: water oxidation catalysis • ruthenium complexes • substitution reactions • kinetics • pentapyridyl ligand

[1] a) N. S. Lewis, *Science* **2016**, *351*, ad19201-aad19209. (b) S. Berardi, S. Drouet, L. Francàs, C. Gimbert-Suriñach, M, Guttentag, C. Richmond, T. Stoll, A. Llobet, A. *Chem. Soc. Rev.* **2014**, *43*, 7501-7519. (c) M. G. Walter, E. L. Warren, J. R. McKone, S. W. Boettcher, Q. Mi, E. A. Santori, N. S. Lewis. *Chem. Rev.* **2010**, *110*, 6446-6473.

[2] (a) P. Garrido-Barros, C. Gimbert-Suriñach, R. Matheu, S. Sala, A. Llobet, *Chem. Soc. Rev.* **2017**, *DOI: 10.1039/c7cs00248c*. (b) L. Tong, R. P. Thummel, *Chem. Sci.* **2016**, 7, 6591-6603. (c) L. Francàs, R. Bofill, J. García-Antón, L. Escriche, X. Sala and A. Llobet, *Molecular Water Oxidation Catalysis: A Key Topic for New Sustainable Energy Conversion Schemes*, John Wiley & Sons Ltd, Chichester UK, 2014. (d) I. Romero, M. Rodríquez, C. Sens, J. Mola, M. R. Kollipara, L. Francàs, E. Mas-Marza, L. Escriche, A. Llobet, *Inorg. Chem.* **2008**, *47*, 1824-1834.

[3] (a) L. Duan, A. Fischer, Y. Xu, L. Sun, *J. Am. Chem. Soc.* **2009**, *131*, 10397-10399. (b) L. Duan, F. Bozoglian, S. Mandal, B. Stewart, T. Privalov, A. Llobet, L. Sun, *Nat. Chem.* **2012**, *4,* 418-423. (c) C. J. Richmond, R. Matheu, A. Poater, L. Falivene, J. Benet-Buchholz, X. Sala, L. Cavallo, A. Llobet, *Chem. Eur. J.* **2014**, *20*, 17282-17286. (d) R. Matheu, M. Z. Ertem, J. Benet-Buchholz, E. Coronado, V. Batista, X. Sala, A. Llobet, *J. Am. Chem. Soc.* **2015**, *137*, 10786-10795. (e) J. Creus, R. Matheu, I. Peñafiel, D. Moonshiram, P. Blondeau, J. Benet-Buchholz, J. García-Antón, X. Sala, C. Godard, A. Llobet, *Angew. Chem. Int. Ed.* **2016**, *55*, 15382-15386.

[4] (a) J. J. Concepcion, J. W. Jurss, J. L. Templeton, T. J. Meyer, *J. Am. Chem. Soc.*, 2008, **130**, 16462-16463. (b) J. J. Concepcion, M.-K. Tsai, J. T. Muckerman and T. J. Meyer, *J. Am. Chem. Soc.*, 2010, **132**, 1545-1557. (c) J. J. Concepcion, J. W. Jurss, M. R. Norris, Z. Chen, J. L. Templeton, T. J. Meyer, *Inorg. Chem.*, **2010**, *49*, 1277-1279. (d) A. Keidel, I. López, J. Staffa, U. Kuhlmann, F. Bozoglian, C. Gimbert-Suriñach, J. Benet-Buchholz, P. Hildebrandt, A. Llobet, *ChemSusChem* **2017,** *10,* 551-561. (f) F. Bozoglian, S. Romain, M. Z. Ertem, T. K. Todorova, C. Sens, J. Mola, M. Rodríguez, I. Romero, J. Benet-Buchholz, X. Fontrodona, C. J. Cramer, L. Gagliardi, A. Llobet, *J. Am. Chem. Soc.*, **2009**, *131*, 15176-15187.

[5] M. Gil-Sepulcre, J. Axelson, J. Aguiló, L. Solà, L. Francàs, A. Poater, L. Blancafort, J. Benet-Buchholz, G. Guirado, L. Escriche, A. Llobet, R. Bofill, X. Sala, *Inorg. Chem.* **2016**, *55*, 11216-11229.

[6] (a) S. Maji, I. Lopez, F. Bozoglian, J. Benet-Buchholz, A. Llobet, *Inorg. Chem.* **2013**, *52*, 3591-3593. (b) R. Zong, R. P. Thummel, *J. Am. Chem. Soc.* **2005**, *127*, 12802-12803. (d) M. Yagi, S. Tajima, M. Komi, H. Yamazaki, *Dalton Trans.* **2011**, *40*, 3802-3804.

[7] (a) A. D. Becke, *Phys. Rev. A* **1988**, *38*, 3098–3100 (b) J. P. Perdew, *Phys. Rev. B* **1986**, *33*, 8822–8824.

[8] S. Grimme, J. Antony, S. Ehrlich, H. Krieg, *J. Chem. Phys.* **2010**, *132*, 154104.

[9] F. Weigend, R. Ahlrichs, *Phys. Chem. Chem. Phys.* **2005**, *7*, 3297–3305.

[10] Y. Zhao, D. G. Truhlar, *JCP* **2006**, *125*, 194101.

[11] S. Grimme, J. G. Brandenburh, C. Bannwarth, A. Hansen, *J. Chem. Phys.* **2015**, *143*, 054107.

[12] (a) J. P. Perdew, K. Burke, M. Ernzerhof, *Phys. Rev. Lett.* **1996**, *77*, 3865 (b) J. P. Perdew, M. Ernzerhof, K. Burke, *J. Chem. Phys.* **1996**, *105*, 9982.

[13] (a) A. D. Becke, *J. Chem. Phys.* **1993**, *98*, 5648–5652 (b) C. Lee, W. Yang, R. G. Parr, *Phys. Rev. B* **1988**, *37*, 785–789.

[14] A. Klamt, G. Schüürmann, *J. Chem. Soc. Perkin Trans. 2* **1993**, *0*, 799–805.

[15] R. Kang, J. Yao, H. Chen, *JCTC* **2013**, *9*, 1872-1879.

[16] J. C. Dobson, T. J. Meyer, *Inorg. Chem.* **1988**, *27*, 3283-3291.

[17] A. C. Sander, S. Maji, L. Francas, T. Boehnisch, S. Dechert, A. Llobet, F. Meyer, *ChemSusChem* **2015**, *8*, 1697-1702.

[18] (a) J. J. Concepcion, J. W. Jurss, M. R. Norris, Z. Chen, J. L. Templeton, T. J. Meyer, *Inorg. Chem.* **2010**, *49*, 1277-1279. (b) D. J. Wasylenko, C. Ganesamoorthy, B. D. Koivisto, M. A. Henderson, C. P. Berlngette, *Inorg. Chem.* **2010**, *49*, 2202-2209. (c) D. J. Wasylenko, C. Ganesamoorthy, M. A. Henderson, B. D. Koivisto, H. D. Osthoff, C. P. Berlinguette, *J. Am. Chem. Soc.* **2010**, *132*, 16094-16106. (d) S. Roeser, P. Farràs, F. Bozoglian, M. Martínez-Belmonte, J. Benet-Buchholz, A. Llobet, *ChemSusChem* **2011**, *4*, 197-207. (e) M. Yoshida, S. Masaoka, J. Abe, K. Sakai, *Chem. Asian J.* **2010**, *5*, 2369-2378. (f) A. Kimoto, K. Yamauchi, M. Yoshida, S. Masaoke, K. Sakai, *Chem. Commun.* **2012**, *48*, 239-241.

[19] S. Sinnechker, A. Rajendran, A. Klamt, M. Diedenhofen, F. Neese, *J. Phys. Chem. A* **2006**, *110*, 2235-2245.

[20] A. V. Marenich, C. J. Cramer, D. G. Truhlar, *J. Phys. Chem. B* **2009**, *113*, 6378-6396.

[21] X. Sala, M. Z. Ertem, L. Vigara, T. K. Todorova, W. Chen, R. C. Rocha, F. Aquilante, C. J. Cramer, L. Gagliardi, A. Llobet, *Angew. Chem. Int. Ed.* **2010**, *49*, 7745-7747.

WILEY-VCH

FULL PAPER

The chlorido ligand in the ruthenium first coordination sphere and a dangling pyridine group enhance water oxidation catalysis by ruthenium pentapyridyl complexes

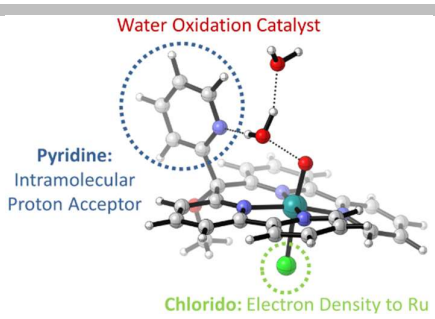

Marcos Gil-Sepulcre, Michael Böhler, Mauro Schilling, Fernando Bozoglian, Cyril Bachmann, Dominik Scherrer, Thomas Fox, Bernhard Spingler, Carolina Gimbert-Suriñach, Roger Alberto, Roger Bofill, Xavier Sala, Sandra Luber, Craig J. Richmond and Antoni Llobet**

Page No. – Page No.

Ru water oxidation catalysts based on py_5 ligands